CHAPTER 4

STUDY OF THE FAILURE AND TOUGHNESS OF SFRC IN SHEAR

4.1. INTRODUCTION

Using steel fibers as shear reinforcement is probably one of the most promising fields for structural applications of SFRC due to the extremely brittle characteristics of the shear failure. Furthermore, such failure is of greater importance when dealing with high strength concrete, which is inherently more brittle than normal strength concrete.

The objective of the present study is to characterize, at the material level, the failure and toughness of SFRC subjected to direct shear loading. With this aim, the push-off test on a double-notched prism has been used to quantify the shear stress-displacement behavior of SFRC. The chosen geometry is similar to that one used by Barr (1986), Swamy (1987), Hsu et. al. (1987), Balaguru and Dipsia (1993), Valle and Buyukozturk (1993), and Khaloo and Kim (1997). This simple geometry seems to give a good approximation of the shear forces that can be transferred across a crack and, consequently, an indication of the shear toughness. Reference tests were also carried out on plain concrete specimens.

4.2. REVIEW OF DIRECT SHEAR TESTS

The failure of plain concrete under shear can be considerably sudden and brittle. Therefore, there has been large interest in determining the response of FRCs under such loading conditions. Several types of specimens have been used (see Figure 4.1) with the objective of producing shear along a prescribed plane (defined normally by cutting notches in the specimen), employing compression and bending loads (Barr, 1987).

An approach that has been quite popular for the estimation of the direct shear response of the material is the push-off specimen (Figure 4.1 a-c), of which different variations have been used (Liu et al., 1985; Barr, 1987; Swamy et al., 1987; Allos, 1989); Benaiche and Barr, 1989; Tan and Mansur, 1990; Balaguru and Dipsia, 1993; Valle and Buyukozturk, 1994). The specimen is basically a prism consisting of two L-shaped blocks that are 'connected' through a ligament along which the shear loading is applied. Other configurations include the punching shear geometry (Figure 4.1 d-e), the Iosipescu beam (Figure 4.1 f) and the confined shear box tests (Figure 4.1 g).

One conceptual aspect that has to be addressed, in discussing shear tests, is the failure mechanism, which appears to be of a tensile nature rather than shear. In most tests, it appears that the failure is basically tensile accompanied by aggregate interlock or fiber bridging.

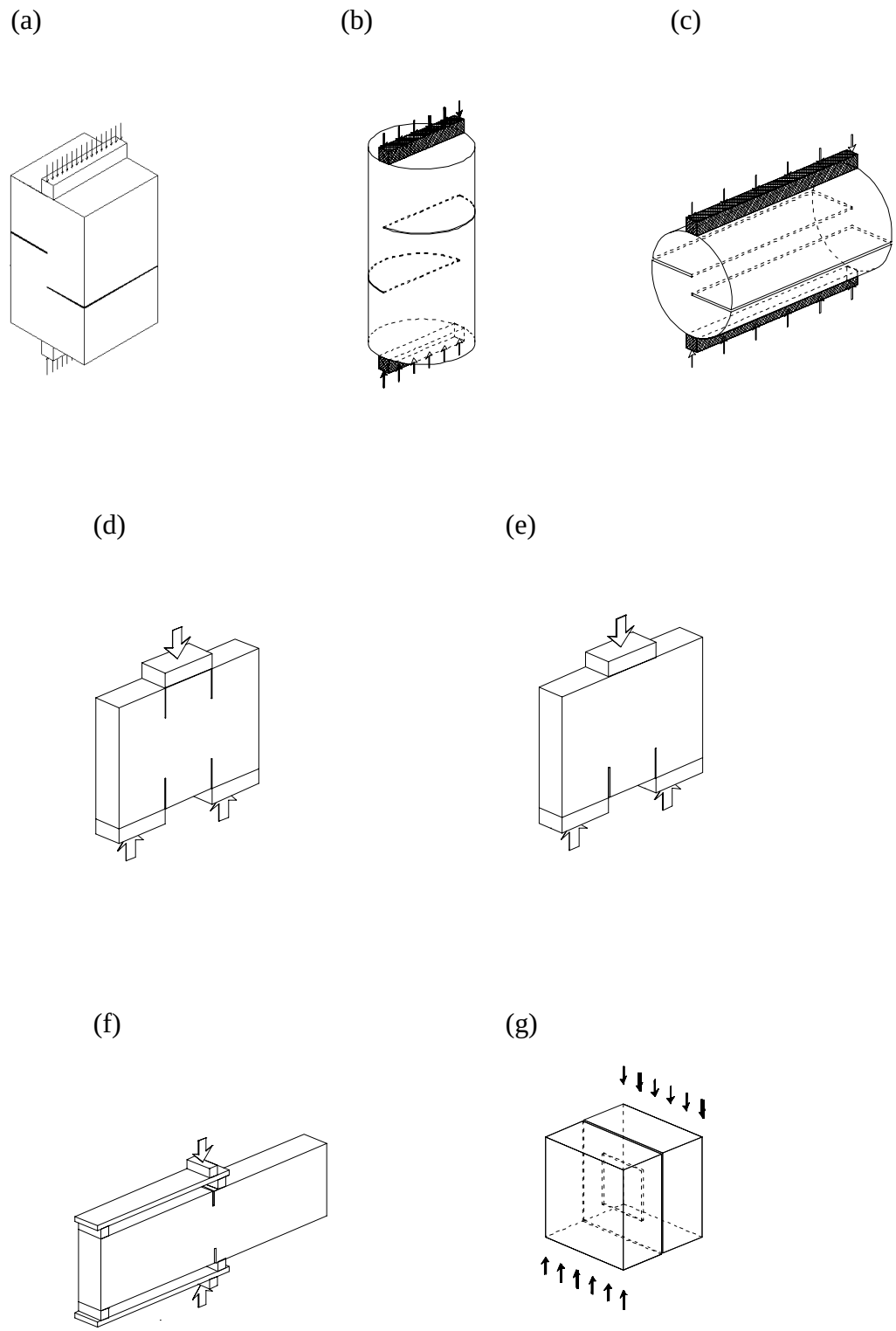

Figure 4.1. Different types of specimens for shear tests

4.3. PROPOSED SPECIMEN GEOMETRY AND TEST SETUP

After a series of preliminary tests with various configurations, such as the width of the loading bar, boundary conditions, mode of control (i.e., piston displacement, horizontal or vertical crack mouth opening displacement) and loading rate, the final dimensions of the specimen were chosen to be those seen in Figure 4.2. The instrumentation of the specimen is given in Figure 4.3.

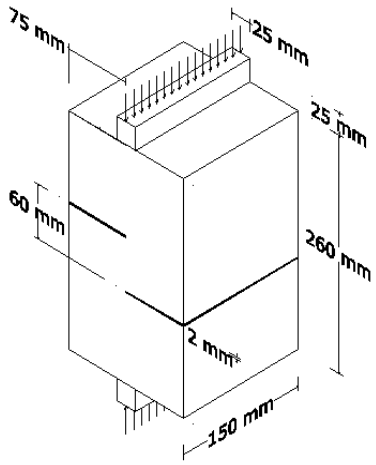

Figure 4.2. Push-off specimen used in the study

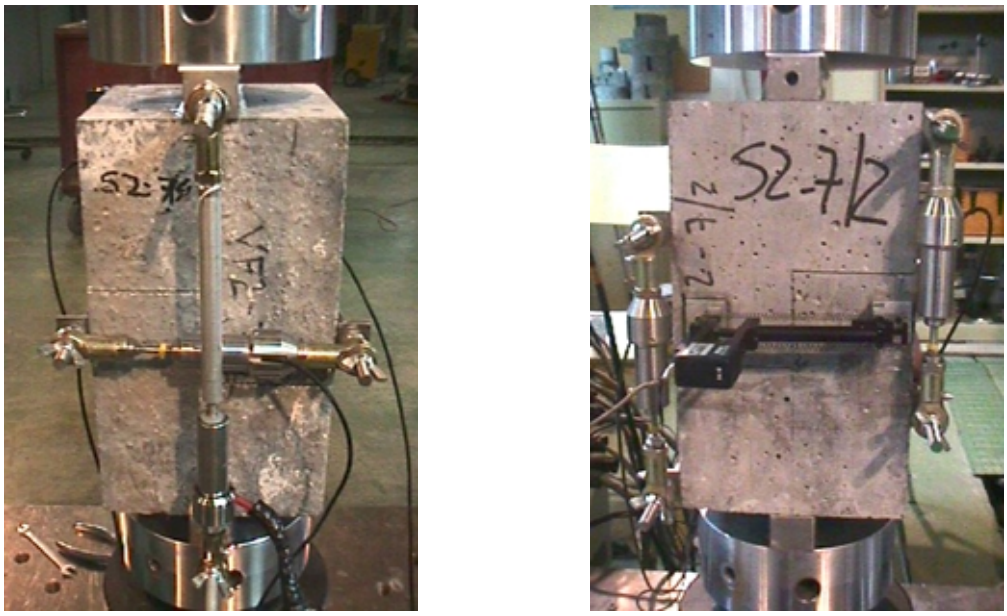

Figure 4.3. General setup

The specimens can be obtained from one of the halves of the notched beams. In the present work, the beams from the tests reported in Annex A were used after cutting away the end that could be affected by the fracture process zone. In other words, from one of the halves of the beams tested in Chapter 2, a core for uniaxial tension was extracted and from the other half a push-off shear specimen was cut (see Figure 4.4).

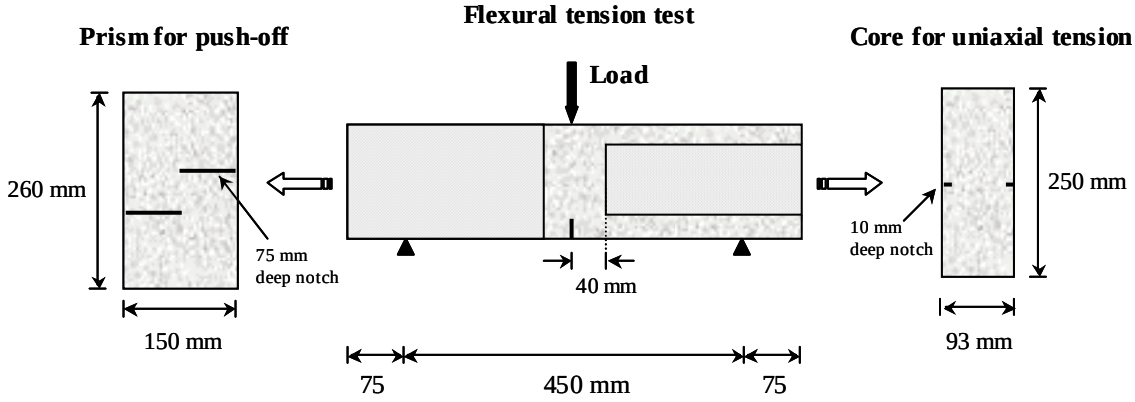

Figure 4.4. Obtention of the push-off specimen

Two notches of 75 mm length were cut, 60 mm apart, perpendicular to the axis of the specimen. The notch-tips define a vertical plane, along which the load is applied. A shear crack is expected to occur along this plane. However, the loading configuration generates tensile stresses along the notch-tip plane. Nevertheless, the shear stresses are about an order of magnitude larger than the tensile stresses (Barr, 1987), and therefore, shear cracking is expected to dominate the failure if the tensile cracking can be controlled. Note that in the present setup, the distance between the notch tips is limited to 60 mm in order to favor shear cracking while maintaining a representative crack plane length.

As it can be seen from Figures 4.2 and 4.3, the load is applied through steel bars of 25 mm width, and 2 mm thick teflon sheets are placed between the fixed loading platens of the machine and the specimen to compensate any unevenness of the loading surfaces. Displacements were measured by means of LVDTs, of 2 mm span, mounted horizontal and vertically on one of the faces of the specimen to measure the respective displacements

(Figure 4.3). The vertical LVDT gives the load-line displacement, which can be taken as the slip once the crack has formed. The horizontal LVDT gives the dilatation of the crack or the crack opening under shear. Additionally, as can be seen from Figure 4.3, on the other face of the specimen, extensometers were placed across the two notches to study the rotation of the crack plane.

The tests were performed in an Instron 8505 servo-hydraulic testing system under closed loop control with a constant piston displacement rate of 0.001 mm/sec, which resulted in the peak load occurring at about 5 minutes and a test duration of approximately 30 minutes. The load and displacements signals from the LVDTs were recorded continuously. Three specimens were tested for each concrete.

Before performing the tests, the geometry of the specimen was analyzed with a finite element program (DRAC, developed by I. Carol and P. Prat at UPC). Simulations were carried out to determine the stress state in the elastic regime. The triangular finite element mesh used in the analysis can be seen in Figure 4.5 and the principal stresses distribution in Figure 4.6, with the blue arrows indicating the direction of the principal compressive stresses and the red arrows indicating the direction of the tensile stresses. It is seen that there are high compressive stresses along the central plane and some tensile stresses predominating in the zones denoted with T, implying the possibility of tensile cracking. The shear stress distribution is shown in Figure 4.7, with red indicating high shear stresses and green indicating low stresses. It can be seen that there are significant shear stresses between the tips of the notches along the shear plane. This suggests that shear failure would occur if tensile cracking is restricted by the fibers. This was confirmed by independent analyses of the same specimens in the Politecnico di Milano (del Giorgio and Trintinaglia, 2000).

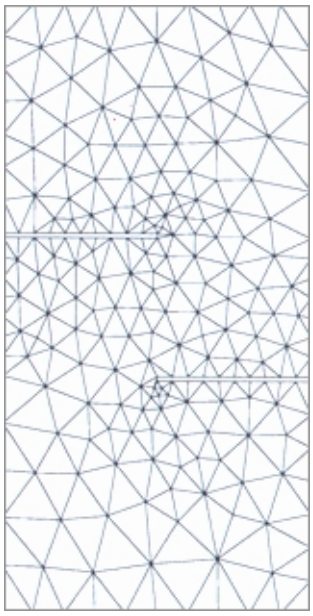

Fig. 4.5

Finite element mesh

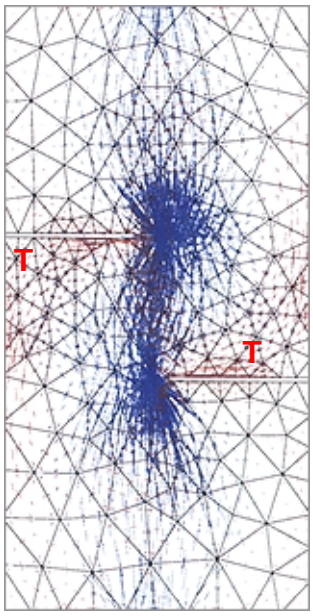

Fig. 4.6

Distribution of principal stresses

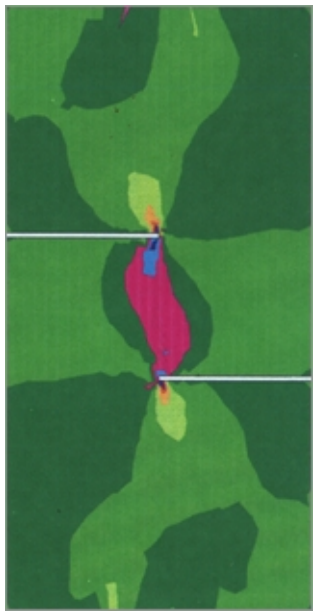

Fig. 4.7

Distribution of shear stresses

This linear numerical analysis was considered sufficient to go ahead with the proposed geometry in terms of experimental testing. Later on section 4.5.1, it will be contrasted with true failure modes observed in experiments.

4.4. MATERIALS STUDIED

Two base concrete mixes have been studied, a normal strength concrete, with a characteristic compressive strength (f_c) of about 35 MPa, denominated C35 (mix N1) and a high strength concrete, designed to achieve an f_c of about 70 MPa, denominated C70 (mix N2). In each mix, 20 and 40 kg/m^3 of steel fibers were incorporated. The characteristics of the materials used, mixes and casting of the specimens are in accordance with the description given in Chapter 2, section 2.5.1 and 2.5.2.

4.5. RESULTS AND DISCUSSION

4.5.1. Failure Modes

The typical mode of failure for the case of plain concrete can be seen in Figure 4.8 and 4.9 for normal and high strength concretes, respectively, which show both sides of the same specimen. The first cracks to appear are the ones marked as 1-2 (see Figure 4.8), which seem to initiate on one of the notch faces, at about 2 cm (i.e., point 1) from the tip and propagate towards the tip of the other notch (i.e., point 2). At about the same time, crack 2-2 appears, which could be defined as a shear crack. Sometimes, only one crack of the 1-2 type appears, followed by almost instantaneous splitting failure. Due to this crack pattern, this test method has been criticized as being inapplicable for obtaining the shear behavior of plain concrete.

Figure 4.8. Typical failure modes for plain NSC (both sides of the same specimen)

Figure 4.9. Typical failure mode for plain HSC (both sides of the same specimen)

The mode of failure in SFRC is significantly different to that of plain concrete, as seen in the typical failure patterns of Figures 4.10 and 4.11 for the cases of NSC and HSC respectively, which show one side of a tested specimen on the left and a closer view of the cracks on the right. Often, failure occurs with the propagation of a single vertical shear crack consisting of a microcracked band that is approximately 1 cm wide. In other cases, there is some secondary cracking; a crack starts at point 1 (see Figure 4.10) and develops to a length of about 1 to 1.5 cm (shown as red lines in Figure 4.10). This crack is later arrested and the principal shear crack develops along plane 2-2. The first crack closes once failure starts to localize on plane 2-2. Individual modes of failures for all specimens tested are presented in Annex E.

It appears that the fibers limit the extent of propagation of the tensile cracks leading to a shear dominated failure in the SFRC. This also justifies the use of the present test methodology to study the shear failure response of fiber concrete, even though it is not entirely suitable for the analysis of such failure in plain concrete.

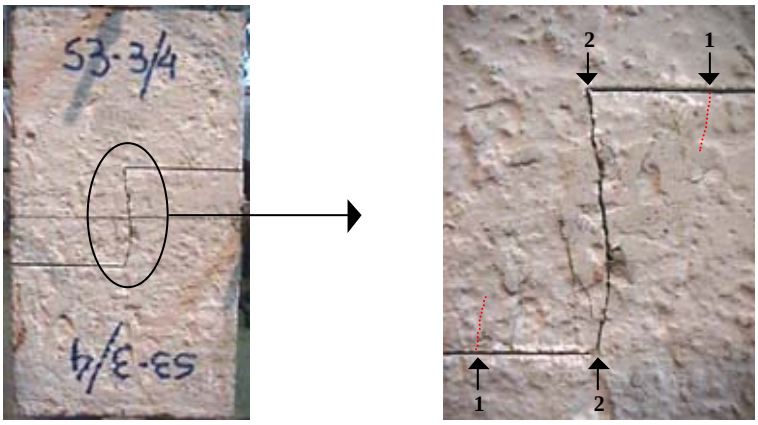

Figure 4.10. Typical failure mode for NS-SFRC (same specimen, closer view on the right)

Figure 4.11. Typical failure mode for HS-SFRC (same specimen, closer view on the right)

4.5.2. Test Response

Figures 4.12 and 4.13 show the typical stress versus vertical displacement (or slip) responses for NSC and HSC, respectively, for plain and fiber concretes. Note that in all calculations of stress, the applied load is divided by the nominal shear plane area of 93.8 cm^2 to obtain a nominal shear stress. Individual test results can be found in Annex E.

For the plain concretes, a practically linear response up to brittle failure can be observed. The behavior of the SFRC specimens is significantly different; the response is linear up to the first-crack (indicated by a peak), followed by a non-linear behavior. After the first peak, the load in the NSC generally decreases gradually indicating the toughening effect of the fibers. In the case of the HSC there is an increase in the stress after the first peak that is more significant for the higher fiber volume.

The maximum shear stresses or strengths, τ_u (mean and coefficients of variations) are given in Table 4.1 for all the concretes. The values clearly reflect the increase in shear strength due to fiber incorporation in the HSC.

In the closer views of the initial responses shown in the plots of the main curves in Figures 4.12 and 4.13, it can be seen that in the case of NSC, the fibers do not influence the behavior up to the maximum load but significantly affect the behavior in the case of HSC.

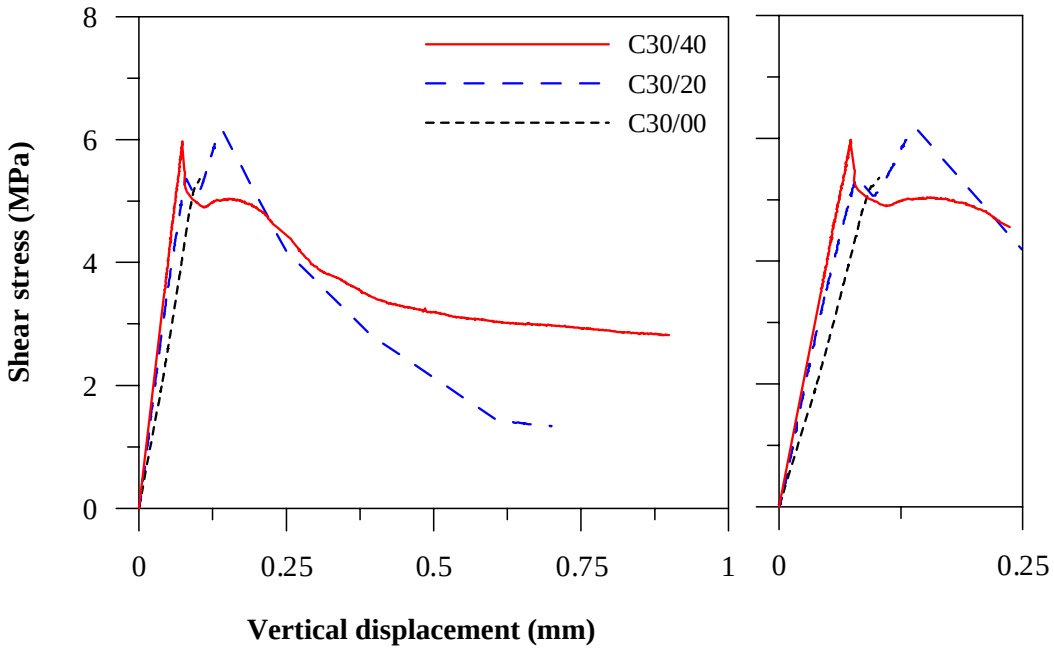

Figure 4.12. Shear stress vs. slip relationship for NSC

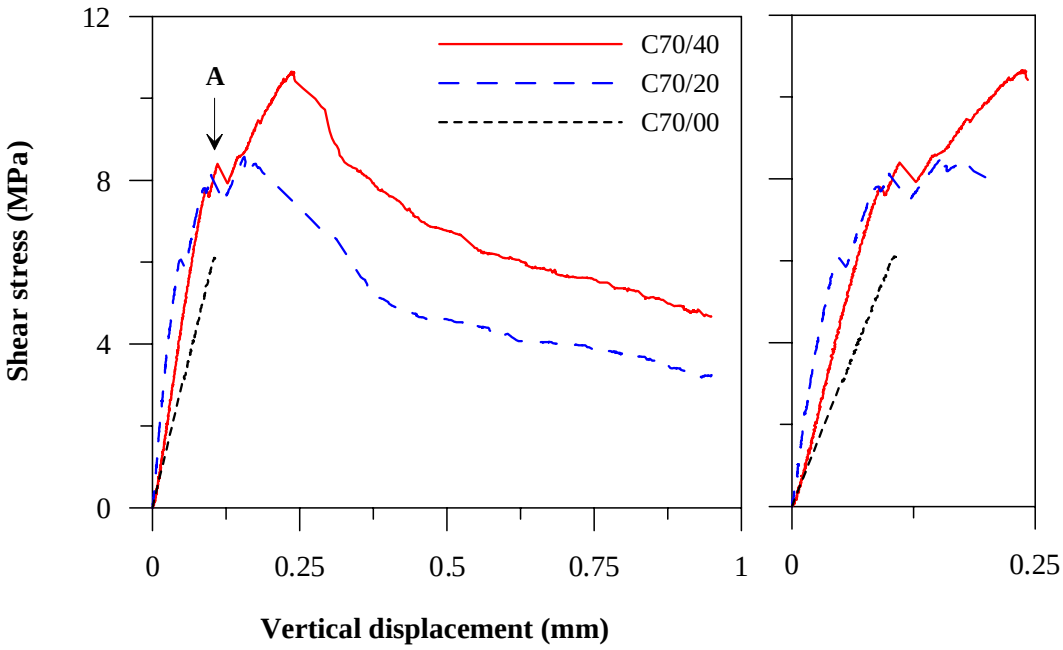

Figure 4.13. Shear stress vs. slip relationship for HSC

Table 4.1. Maximum shear strengths

Concrete	τ_u (MPa)
35/00	4.1 (± 29%)
35/20	6.2 -
35/40	5.9 (± 3%)
70/00	5.5 (± 9%)
70/20	8.2 (± 5%)
70/40	10.0 (± 13%)

Generally, in the SFRC, a gradual decrease in stress can be observed as the slip increases after the peak load with significant residual strengths. This toughening is a result of the pull-out and dowel actions of the fibers.

The improvement of the shear response due to the addition of fibers is influenced by the strength of the concrete and the volume of fibers. In the present work, the higher strength concrete with shorter fibers, which gives more fibers per unit area, yields a better performance. As shown by Walraven, 1994, using push-off specimens with traditional reinforcement or external restraint bars, the reinforcement increases the shear friction capacity in HSCs due to better bond, even though there is higher aggregate rupture. In any case, as can be seen in Figure 4.14, the resisting force due to fiber bridging not only restrains crack opening but also leads to higher interlocking. This, along with the dowel action of the fibers, leads to a lower slip and higher shear transfer.

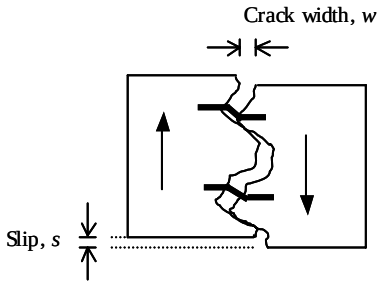

Figure 4.14. Displacement along the cracked shear plane

The failure process can be further explained with the help of Figures 4.15 (typical curves of load vs. slip and crack opening) and Figure 4.16 (corresponding curves of crack width vs. slip). Until point A (i.e., first-crack), the matrix dominates the response, with negligible horizontal displacement, and beyond this point, the horizontal displacement increases or the crack opens. Until the maximum load (i.e., point B), the fibers are progressively activated and the matrix cracks completely. Thereafter, the fracture process localizes in a dilating shear crack band, with the stresses being transferred through the fibers in the post-peak regime. There is a linear relation between the slip and crack opening during this stage.

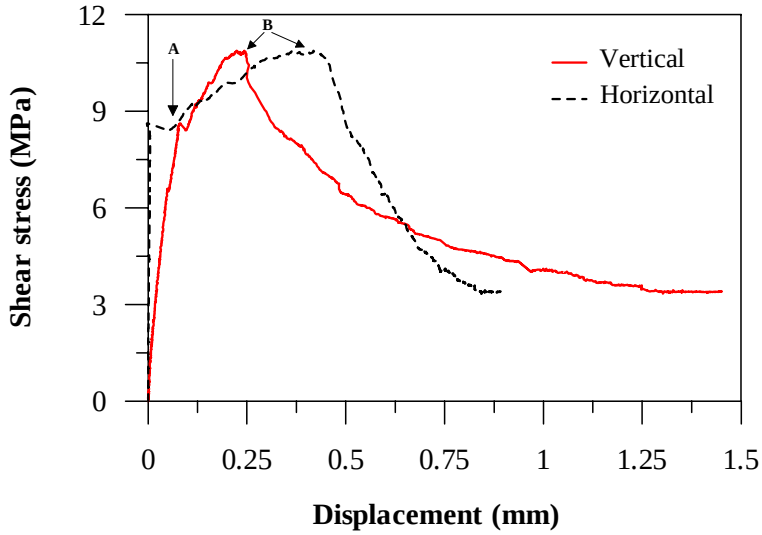

Figure 4.15. Load vs. slip and crack opening relationship

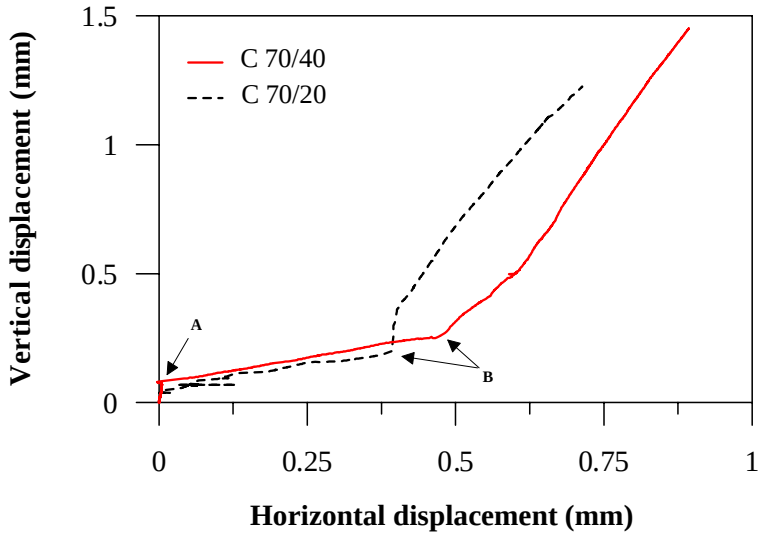

Figure 4.16. Crack width vs. slip relationship

4.5.3. Toughness in Shear Failure

Traditionally toughness is defined in terms of the energy absorbed during the failure of the specimen. This is represented by taking the area under the load-displacement or load-crack opening curve until a certain prescribed limit. An extension of these approaches will allow the definition of shear toughness as the area under the load-slip curve in the push-off test.

4.5.3.1. Absolute Toughness

Firstly, the shear toughness is analyzed considering the absolute toughness $B^{S}_{s_{lim}}$, defined as the area under the stress-vertical displacement response until a certain slip limit (as in Figure 4.17). Its evolution, as the slip increases, can be seen in Figures 4.18 and 4.19. Table 4.2 presents average values up to different slip limits, s_{lim} = 0.25, 0.5 and 1 mm together with the coefficient of variation (COV) in parenthesis. The absence of the COV signifies that the result is an average of two specimens.

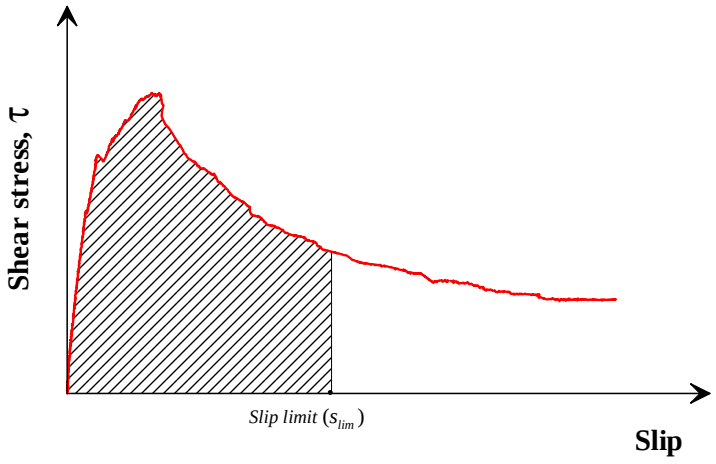

Figure 17. Absolute toughness

Accordingly, the absolute toughness is defined as:

$$B^{S}_{s_{lim}} = \int_{0}^{s_{lim}} \tau^{S}(s)ds \qquad \text{(eq. 4.1)}$$

where τ^{S} is the shear stress at the slip s and s_{lim} is the prescribed slip limit.

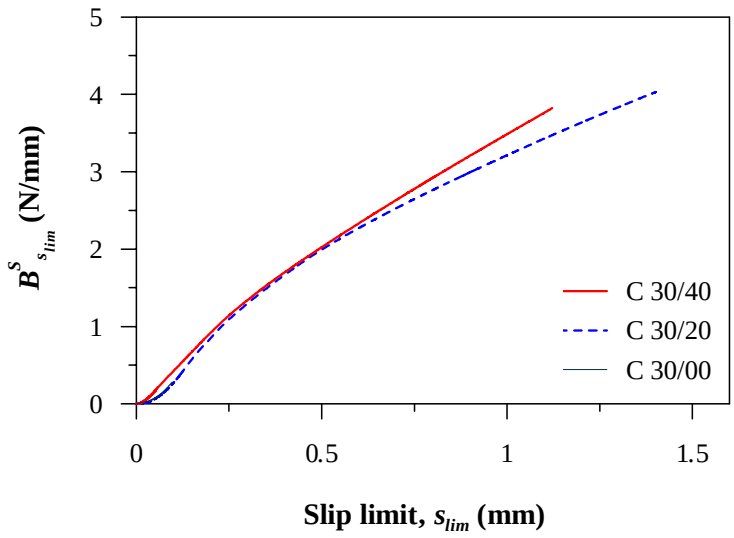

Figure 4.18. Evolution of the absolute toughness with slip limit (for the concrete C 35)

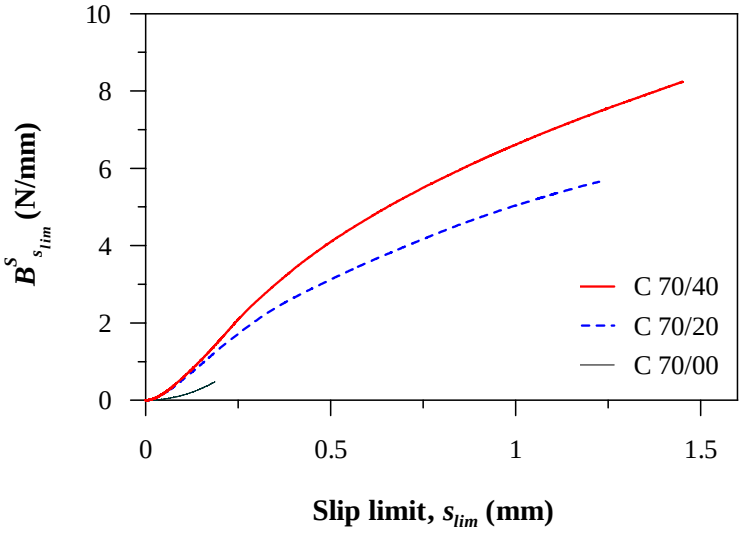

Figure 4.19. Evolution of the absolute toughness with slip limit (for the concrete C 70)

Table 4.2. Absolute shear toughness results

Concrete	**Area under the stress-slip curve,** $B^S_{s_{lim}}$ (N/mm)		
	$B^S_{0.25}$	$B^S_{0.50}$	$B^S_{1.00}$
35/20	1.2 (± 9%)	2.2 (± 11%)	3.7 -
35/40	1.1 -	2.0 (± 3%)	3.8 (± 18%)
70/20	1.7 (± 14%)	2.9 (± 15%)	4.6 (± 14%)
70/40	1.8 (± 16%)	3.6 (± 21%)	6.6 -

From Table 4.2 it can be seen that for the case of NSC (35/20 and 35/40), the absolute toughness does not show a clear increase when 40 kg/m^3 of fibers instead of 20 are added, this is due to the similar shape of the curves in the case of 35/20 concretes (see Figures 4.12, and Annex E). In the case of HSC, the absolute toughness parameter clearly reflects the increase in toughness with an increase in fiber dosage, with higher sensitivity as the slip limit increases. A 45% increase in $B^S_{1.00}$ is achieved when the amount of fibers increases from 20 to 40 kg/m^3.

4.5.3.2. Equivalent Shear Strength

As in the case of flexure, where the equivalent flexural strength as already been introduced in design recommendations for SFRC (RILEM, 2000b), this parameter can be easily calculated also in shear as:

$$f^S_{s_{lim}} = \frac{B^S_{s_{lim}}}{s_{lim}} \qquad \text{(eq. 4.2)}$$

where:

$B^{S}_{s_{lim}}$ is the absolute shear toughness up to a slip limit s_{lim}

Figures 4.21 and 4.22 show typical experimental curves of the $f^{S}_{s_{lim}}$ versus slip limit relationship, which indicate the evolution of the equivalent shear strength with the amount of fibers and concrete strength. The difference in the behavior of the SFRCs is more pronounced in the case of the HSC.

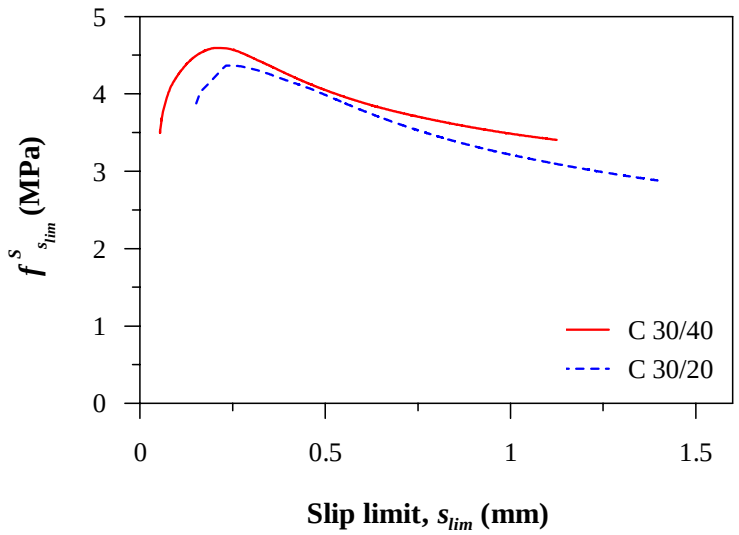

Figure 4.20. Equivalent shear strength vs. slip limit for NSCs

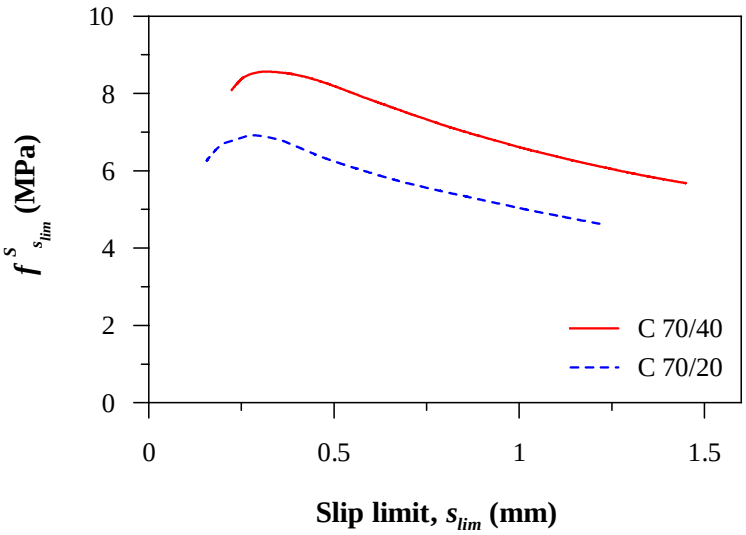

Figure 4.21. Equivalent shear strength vs. slip limit for HSCs

As it can be seen, the curves start after the corresponding peak of the stress–slip relationship since it is not useful to consider an equivalent strength before this point. The shape of the curve shows that the equivalent shear strength has a small increase at the very beginning and then presents a smooth decrease as slip increases. This decrease is due to the continuous softening observed after the peak in the stress–slip relationship (see Figures 4.12 and 4.13).

Average values of equivalent shear strength up to slip limits s_{lim} = 0.25, 0.5 and 1.0 mm are presented in Table 4.6, with the corresponding coefficients of variation in parenthesis. As for absolute toughness, an incorporation of 40 kg/m^3 of fibers in the HSC leads to a 45% increase of $f^S_{1.00}$ with respect to the concrete containing 20 kg/m^3 of fibers.

Table 4.3. Equivalent shear strength results

Concrete	**Equivalent shear strength,** $f^{S}_{s_{lim}}$ (MPa)		
	$f^{S}_{0.25}$	$f^{S}_{0.50}$	$f^{S}_{1.00}$
35/20	4.7 (± 8%)	4.1 (± 18%)	3.7 -
35/40	4.5 -	3.9 -	3.8 (± 18%)
70/20	6.4 (± 12%)	5.9 (± 15%)	4.6 (± 14%)
70/40	7.3 (± 16%)	7.1 (± 21%)	6.6 -

4.5.3.3. Residual Shear Strength

The residual strength is a direct measure of the effective stress that can be transferred across an open crack. Table 4.4 shows the results of the residual strength at the same slip limits considered in the case of absolute shear toughness and equivalent shear strength. As it can be observed, the trends in residual stress values are the same as those observed in the case of toughness parameters. However, in the case of NSC, the improvement in residual strength due to fiber addition can be observed earlier than in the case of toughness parameters, with a 15% increase in $\tau^{0.50}_{res}$ when increasing the fiber dosage from 20 to 40 kg/m^3.

Table 4.4. Residual shear strength results

Concrete	**Residual strength,** $\tau_{res}^{s_{lim}}$ (MPa)		
	$\tau_{res}^{0.25}$	$\tau_{res}^{0.50}$	$\tau_{res}^{1.00}$
35/20	4.7 (± 16%)	2.7 (± 52%)	2.7 -
35/40	4.1 -	3.1 -	3.2 (± 28%)
70/20	6.9 (± 15%)	4.2 (± 15%)	2.6 (± 14%)
70/40	8.7 (± 33%)	5.8 (± 24%)	4.3 -

4.6. CONCLUSIONS

Tests of notched specimens in the push-off configuration, demonstrate the energy dissipation capacity of steel fiber reinforced concrete in the post-cracking regime. The incorporation of fibers in concrete subjected to shear leads to a better mechanical integrity during failure. Moreover, the dowel action of the fibers can lead to considerable residual load-carrying capacity in shear-dominated failure.

Significant improvements in the ductility of concrete during shear failure and some increase in the shear strength are achieved through the incorporation of steel fibers in both normal and high strength concretes. However, this improvement is much more important in the case of HSCs, due to the better fiber-matrix bond and the use of high carbon content steel fibers.

The push-off test can give an estimation of stress-based toughness parameters, including the residual and equivalent shear strengths of the open crack. This may allow the use of such parameters in shear design.